Nanoscale

PAPER

View Article Online
View Journal | View Issue

Cite this: *Nanoscale*, 2022, **14**, 8069

On-surface synthesis of Mn-phthalocyanines with optically active ligands†

Amelia Domínguez-Celorrio, [a,b] Carlos Garcia-Fernandez,[c,d] Sabela Quiroga,[e] Peter Koval,[f] Veronique Langlais,[b] Diego Peña, [e] Daniel Sánchez-Portal,[c,d] David Serrate *[a,g,h] and Jorge Lobo-Checa *[a,g]

Received 7th February 2022,
Accepted 26th April 2022

DOI: 10.1039/d2nr00721e

rsc.li/nanoscale

The synthesis of novel organic prototypes combining different functionalities is key to achieve operational elements for applications in organic electronics. Here we set the stage towards individually addressable magneto-optical transducers by the on-surface synthesis of optically active manganese-phthalocyanine derivatives (MnPc) obtained directly on a metallic substrate. We created these 2D nanostructures under ultra-high vacuum conditions with atomic precision starting from a simple phthalonitrile precursor with reversible photo-induced reactivity in solution. These precursors maintain their integrity after powder sublimation and coordinate with the Mn ions into tetrameric complexes and then transform into MnPcs on Ag(111) after a cyclotetramerization reaction. Using scanning tunnelling microscopy and spectroscopy together with DFT calculations, we identify the isomeric configuration of two bi-stable structures and show that it is possible to switch them reversibly by mechanical manipulation. Moreover, the robust magnetic moment brought by the central Mn ion provides a feasible pathway towards magneto-optical transducer fabrication. This work should trigger further research confirming such magneto-optical effects in MnPcs both on surfaces and in liquid environments.

I. Introduction

Organic electronic devices are nowadays an industrial reality due to their high efficiency, low-cost and synthetic design tunability.[1–3] Among them, phthalocyanines (Pcs) and porphyrins stand out as prototypical examples of organic semiconductor building units due to their electric, magnetic and optical adjustability by metallation of their central cores.[4] These metal–organic complexes are used as pigment catalysts and photo-sensitive semiconductors besides being promising candidates for molecular spintronic applications.[5,6]

When organic complexes are adsorbed on surfaces, important interfacial interactions emerge that influence their electronic and magnetic properties.[5–7] In the case of metallated Pcs and porphyrins with first-row transition-metal (TM) ions, significant conformational and spin state modifications have been reported.[7–10] These are strongly dependent on the local adsorption sites of metal centers and the arrangement of their external ligands, which alter the relative position of the metal center with respect to the π-conjugated macrocyclic plane. Similarly, selective adsorption of external and axial ligands on the metal centers modify these metal–organic complex properties.[11–14] Such local variability limits the scalability of single-molecule device production since building blocks require dynamical control and operational reversibility while maintaining their overall chemical and physical environments.

A way to overcome these local conformation limitations could be inserting active molecular switches into molecular complexes so that morphological control can be exerted using external stimuli, in the form of photons,[15,16] focused electric fields[17,18] or electric currents.[19,20] Light illumination is particularly simple to technically control, but demands that the spin centers of molecular complexes are strongly coupled to switchable ligands whose conformations can be changed by photon adsorption. The synthesis and deposition on the sur-

[a]*Instituto de Nanociencia y Materiales de Aragón (INMA), CSIC-Universidad de Zaragoza, Zaragoza 50009, Spain. E-mail: serrate@unizar.es, jorge.lobo@csic.es*
[b]*Centre d'Elaboration de Materiaux et d'Etudes Structurales – Centre National de la Recherche Scientifique, Toulouse, France*
[c]*Centro de Física de Materiales CSIC/UPV-EHU-Materials Physics Center, Manuel Lardizabal 5, E-20018 San Sebastián, Spain*
[d]*Donostia International Physics Center, Paseo Manuel de Lardizabal 4, E-20018 San Sebastian, Spain*
[e]*Centro de Investigación en Química Biolóxica e Materiais Moleculares (CIQUS), Departamento de Química Orgánica, Universidade de Santiago de Compostela, Santiago de Compostela 15782, Spain*
[f]*Simune Atomistics S.L., Avenida Tolosa 76, 20018 San Sebastian, Spain*
[g]*Departamento de Física de la Materia Condensada, Universidad de Zaragoza, E-50009 Zaragoza, Spain*
[h]*Laboratorio de Microscopías Avanzadas, Universidad de Zaragoza, E-50018 Zaragoza, Spain*
† Electronic supplementary information (ESI) available. See DOI: **https://doi.org/10.1039/d2nr00721e**

faces of such magnetic and optically active molecules by direct thermal evaporation is still pending, as it is compromised by the structural fragility of these metal–organic complexes. Such molecular integrity limitation has prevented its fabrication and implementation into magneto-optical transducers.

In this work, we achieved an adequate strategy to create metal–organic complexes by on-surface synthesis (OSS) featuring optically active moieties. In particular, we generated active Pcs with a central magnetic atom by means of cyclotetramerization of a functionalized phthalonitrile precursor on the Ag(111) surface. We chose Mn atoms as metallic centers based on their expected magnetic response that is evidenced in their reported Kondo signals on Ag substrates.[21,22] We find that the produced manganese phthalocyanines (MnPcs) have the central magnetic ions coupled to four diarylethylene (DAE) moieties. These MnPcs on Ag(111) show at each branch two possible conformations that we image and study electronically by scanning tunneling microscopy (STM) and spectroscopy (STS) techniques. Density functional theory (DFT) calculations allow us to identify the relevant configurations of the open and closed DAE isomers on the Ag(111) surfaces, and confirm the robust magnetic moment localized at the Mn ion. Notably, we induce reversible changes between the open and closed conformations by lateral tip-molecule manipulation. Although magneto-optical experiments were not attempted here, this OSS process ensures that each MnPc we formed contains four switchable branches.

II. Results and discussion

Optical activity of precursor 1

As a molecular precursor we designed and synthesized 4,5-bis(benzo[*b*]thiophen-3-yl)phthalonitrile that we name hereafter compound **1a**. This compound was obtained in two steps by solution chemistry from commercially available compounds (see the ESI† for details). Compound **1a** includes two vicinal nitrile (CN) groups to induce the on-surface cyclotetramerization reaction leading to phthalocyanine. It presents two vicinal benzothiophene groups forming a diarylethene moiety that should be involved in a reversible electrocyclization reaction leading to compound **1b** (closed isomer), *i.e.* these moieties are introduced as an active switchable structure.[23]

When a UV light of 365 nm wavelength irradiates a solution of compound **1a** in CH_2Cl_2, the optical activity is photochromatically evident: the initial colorless solution corresponding to the open isomer **1a** changes into blue as these molecules transform into the closed isomer **1b** (Fig. 1a). The photochemically induced electrocyclic reaction involves six π-electrons, and therefore, according to the Woodward–Hoffmann rules the cyclization should be conrotatory, giving product *trans*-**1b**. The isomerization is reversible since the solution changes back to colorless once the UV irradiation is stopped (see ESI Fig. S1†).

Dehydrogenation of the closed isomer **1b** leads to the formation of conjugated dicyanonaphthalene **2** (Fig. 1b), which does not vary its color in solution when irradiated with the same UV light. Its unique isomeric configuration and planar geometry will be used as a control to ensure the presence of the optically active ligands of **1**.

Integrity and isomeric configurations of 1 and 2 upon Mn co-deposition on Ag(111)

Isomeric molecules exhibiting active reversible switching have already been reported on metal surfaces responding to different stimuli, *e.g.* photons,[15,16] electrons[19,20] or electric fields.[17,18] These delicate ligand groups can withstand UHV evaporation whenever the molecules are small, since this permits sublimation at low enough temperatures that preserve their integrity. By contrast, larger molecules containing heavier metal centers tend to break apart at the active (and weakest) end groups.

The pathway that could lead to the generation of magneto-optical transducers requires to fulfill two conditions: first, deposition of optically active precursors that preserve their moiety integrity and, second, their combination with magnetic atoms. To achieve this, we evaporated small, optically active precursor molecules under UHV conditions so they self-assemble with Mn atoms on Ag(111). This surface is then used to catalyze a more complex structure by OSS. In order to prevent the Mn from clustering, we simultaneously deposited Mn atoms and precursor **1a** on a Ag(111) surface kept at 50 °C (see the Methods section in the ESI†). As shown in Fig. 2a, squared-lattice islands are formed by the self-assembly of tetramer units that consist of Mn atoms (imaged as dark depressions) coordinated to four molecules by their cyano groups.[24,25] These metal–organic tetramers are quite stable since they conserve their integrity after lateral atomic manipulation with an STM tip (see the inset of Fig. 2a). The islands of Mn + four **1a** ligands are stabilized by the formation of hydrogen bonds with adjacent molecules (see Fig. S2†). In the coordinated islands, STM topography reveals two types of asymmetric ligands with different external lobes, also found for other diaryl derivatives on Ag(111).[26] For convenience, we will refer to the brighter lobes as *A*-configuration and the darker lobes as *B*-configuration (*cf.* red and green arrows in the inset of Fig. 2a). These lobes are randomly distributed and for an island with 452 molecules of **1** we find an *A*/*B* ratio of 0.72, as if the interactions between neighboring tetramer units were independent of their external conformations. This randomness suggests that both configurations are structurally very similar, as expected from the two isomers **1a** and **1b** sketched in Fig. 1a.

An identical process of co-depositing Mn + compound **2** on Ag(111) leads to very different structures. The similarity with the previous metal–organic complex is restricted to the formation of coordinated units of Mn atoms and four molecules by their cyano groups[24,25] (*cf.* Fig. 2b). However, these complexes are monodispersed and do not self-assemble into islands. Moreover, the ligands do not present visible differences in the external groups. We assign the absence of island aggregation to the lack of the two additional hydrogen atoms

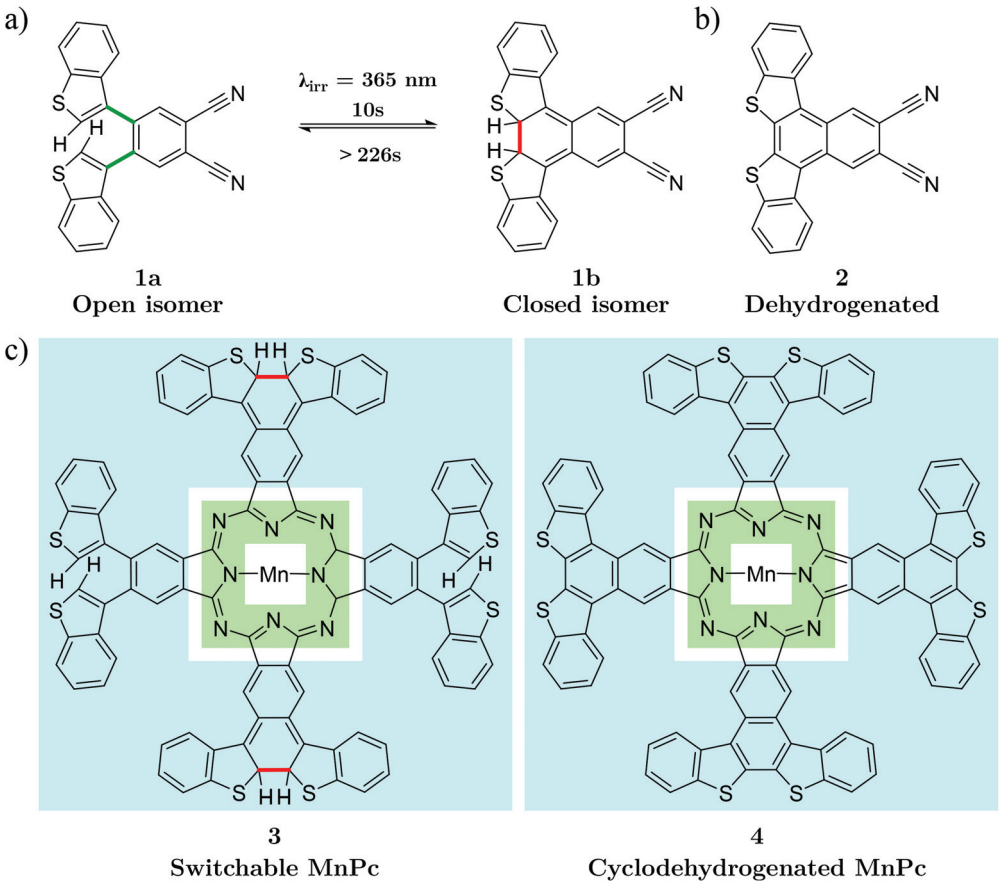

Fig. 1 Molecular precursors and MnPc complexes of this work. (a) Scheme of the reversible reaction between open **1a** and closed **1b** isomers. (b) Molecular structure of the fully conjugated and non-switchable precursor dicyanonaphthalene **2** used for verification. (c) Molecular structure of the MnPcs synthesized by cyclotetramerization reactions. Complex **3** is generated from **1** and presents four switchable DAE moieties, whereas **4** is a rigid MnPc produced from **2**. Green shading marks the identical phthalocyanine rings containing the central Mn, while blue denotes the bisbenzothiophene moieties.

at their external DAE moieties compared to **1a** and to the enhanced structural conjugation of the **2** precursors. All these findings confirm the molecular integrity of both **1** and **2** on the Ag(111) surface and the coordination with Mn into tetramer units that sets the stage for the MnPc formation by OSS.

MnPc formation by cyclotetramerization of metal–organic complexes

Post-annealing of these Mn complexes leads to the cyclotetramerization process of the ligands around the Mn atom[24,25,27] (see the Methods section in the ESI†). The cross shape observed in STM (*cf.* inset Fig. 2c) follows the MnPc structure sketched in Fig. 1c with four branches associated with the precursor molecules. Interestingly, the central Mn is now imaged as a bright protrusion, implying a significant electronic reconfiguration after the annealing process. The synthesized switchable MnPcs (**3**) still arrange into squared self-assembled islands (Fig. 2c), whereas the conjugated MnPcs (**4**) continue to be spread out on the surface (Fig. 2d). This difference should relate once again to the presence or absence of hydrogen atoms at the bisbenzothiophene moieties.

Focusing on **3**, from the high resolution images of individual molecules extracted from the island by atomic manipulation (Fig. 3a–d), we still identify two apparent configurations of the peripheral DAE groups. We keep naming *A* for the brighter lobes (*e.g.* top branch in Fig. 2c inset) and *B* for the darker ones. These lobes must correspond to different benzothiophene arrangements since these two configurations are randomly present in the MnPc branches. These MnPcs (**3**) are far from being planar, with *A* lobes being further corrugated than *B* lobes. Indeed, recording constant-height and bond-resolved images with a functionalised CO-tip (see Fig. S3†) is only feasible by vertically adjusting the tip height for each kind of lobe. Interestingly, the external branches in **3** do not show mirror symmetry with respect to their adjacent pyrrole ring (see Fig. 3). The superimposed chemical structure on a switchable MnPc with two *A* and two *B* branch configurations duplicated in Fig. 3c and d includes the branch configurations with the lowest energies (see DFT calculations in Table 1). The *open-rot* configuration fails when fitting the underlying topo-

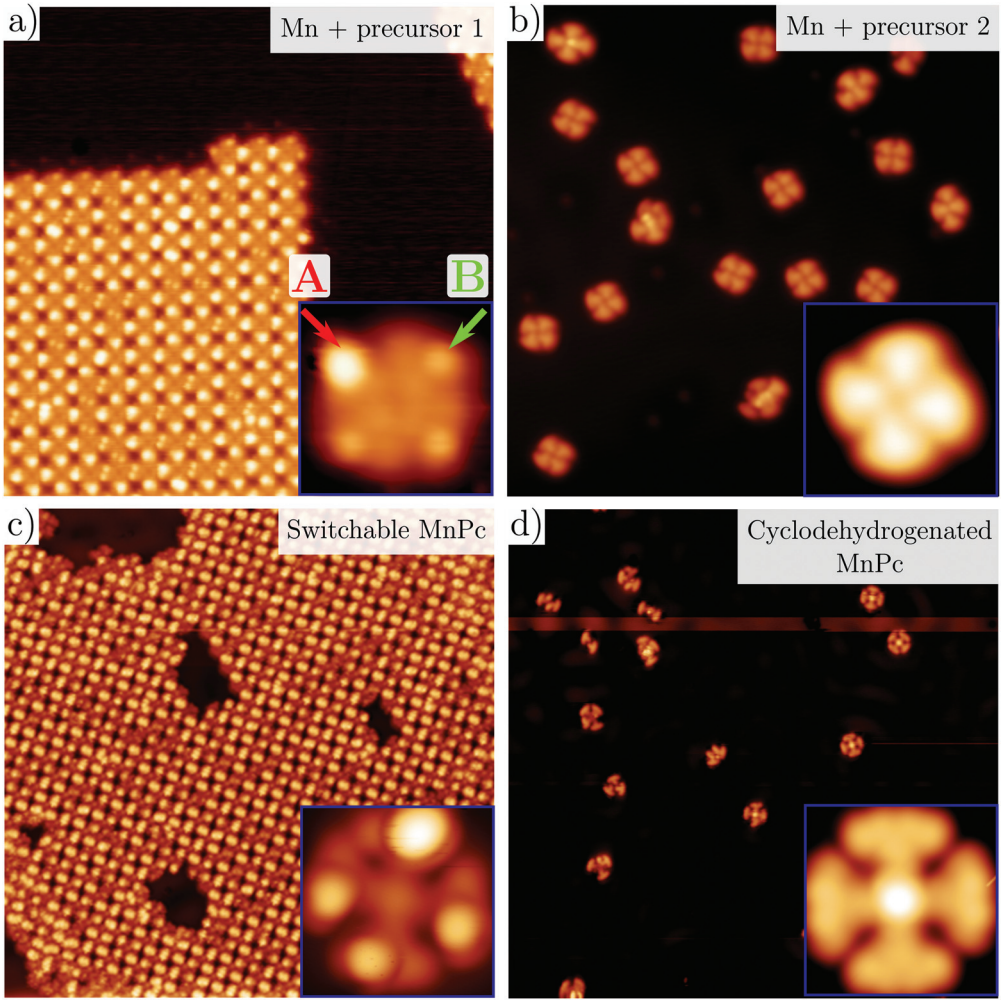

Fig. 2 Representative STM images of the metal–organic structures. (a) Survey and closeups of precursors **1a** (a) and **2** (b) co-evaporated with Mn atoms on Ag(111). Each Mn atom is surrounded by four ligands forming stable metal–organic coordination units. In contrast to (b), the Mn + **1** units cluster into islands (see the molecular model in Fig. S2†) where each complex with four ligands can be manipulated and extracted without damage (*cf.* inset). The DAE moieties present two types of lobes (named *A* and *B*) which are marked by red and green arrows in the inset. Post-annealing the above structures to ~300 °C and ~350 °C induces cyclotetramerization of the ligands forming the MnPcs **3** (c) and **4** (d), respectively. As evidenced in the insets, the Pc core in **3** displays branches with two distinct appearances, whereas **4** is fully conjugated and structurally flat in comparison (see bond-resolved STM images in Fig. S3†). STM images: (a) 40 × 40 nm^2, 0.6 V, 60 pA, inset (a) 3.5 × 3.5 nm^2, 0.6 V, 60 pA; (b) 40 × 40 nm^2, −1 V, 100 pA, inset (b) 3.5 × 3.5 nm^2, −1 V, 100 pA; (c) 50 × 50 nm^2, 10 mV, 50 pA, inset (c) 2.5 × 2.5 nm^2, 0.4 V, 100 pA; and (d) 50 × 50 nm^2, 10 mV, 50 pA, inset (d) 2.5 × 2.5 nm^2, −0.4 V, 20 pA.

graphic STM footprints both for *A* and *B* lobes at the red arrows (*cf.* Fig. S4†). In contrast, the molecular models for open and closed configurations in Fig. 3d satisfactorily reproduce the observed topography.

By contrast, the cyclotetramerized molecules **4** in Fig. 2d† present four similar and symmetric branches with a rather homogenous intensity distribution. The formation of a cyclodehydrogenated MnPc with its expected planar structure is confirmed by bond resolved STM images (see Fig. S3†), corroborating the cyclotetramerization reaction process of these MnPcs on the surface. Moreover, the differences in the STM images of **3** confirms the integrity of DAE moieties in the latter, based on the *A*/*B* branch lobe detection that maintains a bimodal distribution.

Electronic structure by STS of the switchable MnPc

The identified *A*/*B* conformers in the four branches of **3** must have associated with different electronic states, even if they are isomers. To confirm this, we acquired constant height differential tunneling conductance (d*I*/d*V*) spectra at selected positions on several individual molecules extracted from a compact island (see Fig. 4a). For the *B* lobe (darker branch), we observed two occupied states at −1.3 V and −0.3 V, an increase of the conductance around 0.41 V and two clearly resolved peaks at 1.6 V and 2.3 V. This is in contrast to the rather featureless *A* branch spectrum in this energy range, which presents its dominant peak at 3.1 V (see ESI Fig. S5†). Such electronic differences between branches are evident in the topo-

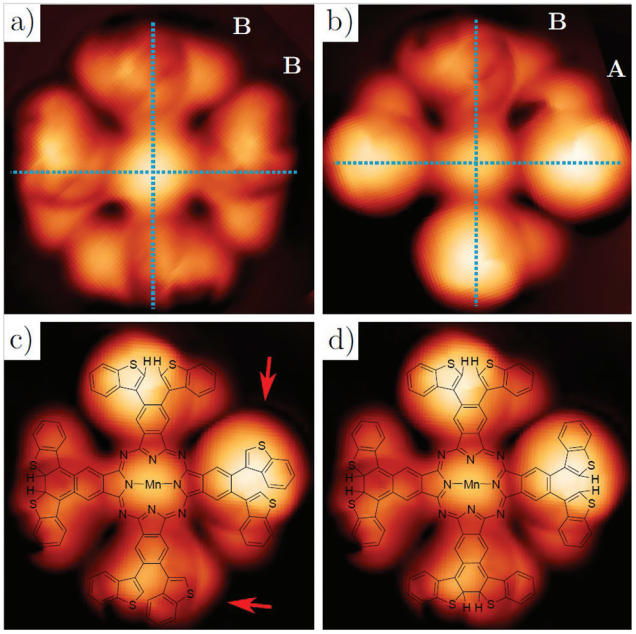

Fig. 3 High resolution imaging and DFT structural models of **3**. (a)–(c) STM images with a functionalized tip (2.5 × 2.5 nm^2, −50 mV, 20 pA) of three different switchable MnPcs (**3**) isolated by lateral atomic manipulation (manipulation set point 5 mV and 15–40 nA). (d) is duplicated from (c) to compare two different superimposed molecular models from the three DFT branch configurations (see Table 1 and Fig. S4†). The positions where the model does not fit their underlying topographic STM footprints are indicated by red arrows in (c). This corresponds to the *open-rot*, which does neither fit *A* nor *B* lobes (*cf.* Fig. S4†). The correct molecular structure is overlaid in (d). The perpendicular dotted lines in (a) and (b) indicate the symmetrical axis expected for square-planar molecules.

graphic images and the d*I*/d*V* map at −1.3 V (Fig. 4b and e). The HOMO–LUMO gap is significantly smaller for the *B* branch (0.7 eV) than for the *A* branch, as can be expected for the closed isomer. Interestingly, the Mn spectrum is independent of the configuration of the branches and presents a sharp peak right below the Fermi level with a ∼50 mV linewidth and a broad resonance at 2.3 V.

DFT calculations of isomeric MnPc (3) adsorbed on Ag(111)

At this point we must correlate the *A* and *B* electronic structures of the DAE moieties of **3** with their atomic arrangement. To do so, we performed DFT calculations of fully relaxed isomeric MnPc on a 9 × 10 × 3 Ag(111) supercell setting an equal atomic arrangement to the four branches (see the Methods section in the ESI†). Table 1 shows the relative energies of the three most stable configurations, where the minimum corresponds to the *open* arrangement (one sulfur atom pointing towards the surface and the other away from it). The second most favorable configuration is the *open-rot* that features a benzothiophene group rotated around its σ-bond by about 195° so that both sulphur atoms point to the surface. The third most stable configuration is the *trans-closed*, where the external hydrogen atoms are vertically opposed with respect to the MnPc central plane (one pointing towards the surface and the second away). Another identified possible configuration is the *cis-closed* isomer (see Fig. S8†), where both hydrogen atoms point away from the surface. Note that this structure confers a distinct mirror symmetry to the branch, which was experimentally absent.

These DFT atomic arrangements must agree with the STM/STS datasets. We can start by discarding the symmetric *cis-closed* arrangement shown in Fig. S8† since none of the branches of **3** exhibits mirror symmetry with respect to the pyrrole ring (*cf.* Fig. 3a–d). In a similar way, the more compressed structural model of the *open-rot* isomer (superimposed to the MnPc in Fig. 3c) does not match the topographic STM footprint neither for *A* nor *B* lobes. Not only is energetically less stable than the *open* configuration, but it also shows almost identical LDOS for the molecular orbitals near the Fermi level (see ESI Fig. S9†). Thus, it is justified to rule out the presence of the *open-rot* isomer and restrict our external atomic arrangements to the *trans-closed* and *open* configurations. Their sideview comparison in Table 1 shows a larger apparent height and a more pronounced asymmetry for the latter, which agrees with the corrugation found in the constant-current images in Fig. 3. Consequently, we associate the *open* arrangement with the *A* configuration and the *trans-closed* with the *B* lobes.

To further increase the confidence in the assignment of the atomic arrangements of *A*/*B* lobes we calculated the local density of states (LDOS) in the energy window (−1, −0.5) eV corresponding to the highest fully occupied molecular orbital of **3** with four identical branches. The resulting LDOS for the *open* and *trans-closed* MnPcs is shown in Fig. 4c and d. The *open* branched MnPc exhibits a higher electronic density mainly localized at the pyrrole rings, whereas the *trans-closed* shows more weight towards the external branches. Moreover, our calculated PDOS (see ESI Fig. S9†) support a shift to lower energies in the HOMO position for the *trans-closed* structure due to a higher conjugation of its branches with the pyrrole ring center. Then, based on this feature of the HOMO, we correlated the calculated molecular orbital of Fig. 4d for the *trans-closed* geometry with the experimental d*I*/d*V* signal observed at −1.3 V of Fig. 4e. In contrast to constant current images, the darker *B* branches (number 4 in Fig. 4b) display a dominant character in the charge density distribution in the d*I*/d*V* maps of occupied states. Indeed, the *trans-closed* intensity maximizes closer to the sulfur atoms for the HOMO (*cf.* Fig. 4e). In contrast, the *A* branches (numbers 1, 2 and 3 in Fig. 4b) featuring brighter signals in the constant current, become practically irrelevant and only reflect the higher corrugation inherent to the *open* configuration in the d*I*/d*V* map. The LDOS of this occupied molecular orbital qualitatively agree with the features described for the calculated HOMO shown in Fig. 4c.

Isomer branch switching by mechanical manipulation

After identifying these two *A*/*B* configurations, we must demonstrate the feasibility of switching between the *open* and

Table 1 DFT calculations of the isomeric MnPc structures of **3** adsorbed on Ag(111). After force relaxation, three atomic arrangements are identified (based on identical branch configurations) when adsorbed on Ag(111): *open*, *open-rot* and *trans-closed*. The minimum total energy structure corresponds to the *open* configuration and is used as a reference for the other cases. The last two columns indicate the maximum vertical separation omitting the hydrogen atoms (Δh_{max}) and Mn ion distance (Δz_{Mn}) relative to the open configuration and with respect to the last Ag slab of the surface. The insignificant differences in the Mn height result in practically identical total magnetic moments. The last two bottom rows show the chemical models of the corresponding branch configurations and the DFT calculated side views on a Ag(111) substrate (with the back branch removed for visualization purposes). A fourth conformation, the *cis-closed* configuration (shown in Fig. S8†), was identified and immediately discarded due to the experimental absence of fully symmetric branches

Isomeric MnPc	Total energy (eV)	Total magnetic moment (μ_B)	Δh_{max} (Å)	Δz_{Mn} (Å)
Open	0	1.91	0.00	0.00
Open-rot	0.02	1.95	0.90	0.01
trans-Closed	0.67	1.89	−1.50	−0.04

Open *Open-rot* *trans-closed*

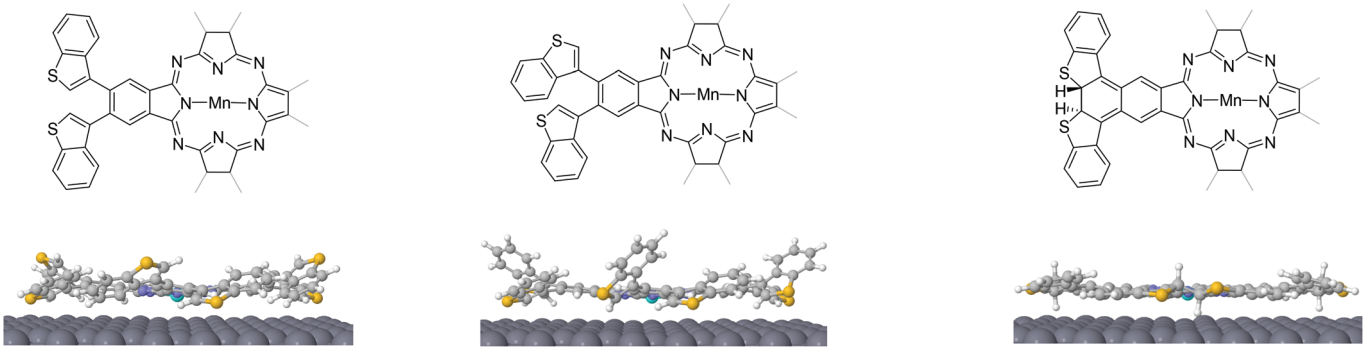

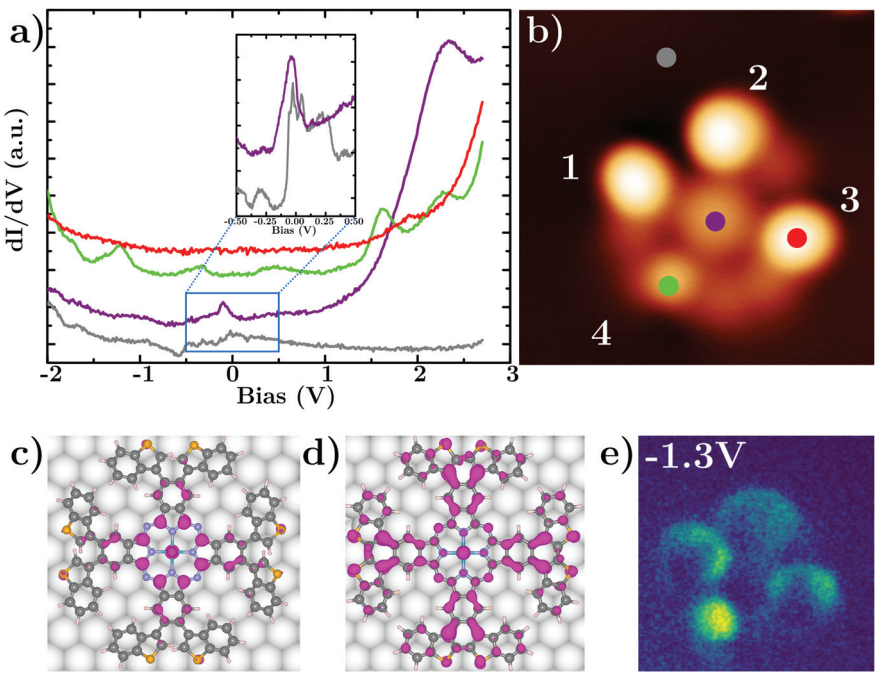

Fig. 4 Experimental and calculated electronic structures of **3**. (a) Position dependent d*I*/d*V* spectra (V_{mod} = 10 mV) recorded at representative points on several isomeric MnPcs: Mn is shown in violet, the *A* lobe in red, the *B* branch in green and the substrate reference in gray. (b) Constant current STM image (V = −50 mV, I = 20 pA, 3.5 × 3.5 nm^2) with color dots indicating the reference positions of the STS in (a). (c) and (d) LDOS calculated isosurfaces of **3** for the highest fully occupied molecular orbital in the energy window (−1, −0.5) eV with the four branches in *open* (c) and *trans-closed* (d) atomic arrangements. The electronic density becomes more delocalized over the external branches on the *trans-closed*, indicative of conjugation at the external branches in comparison to the *open* configuration. (e) d*I*/d*V* map at −1.3 V (V_{mod} = 10 mV) corresponding to (b), showing the spatial distribution of the occupied states.

trans-closed configurations without destroying the molecule. We can do so by lateral atomic manipulation over the Ag surface. We observed frequent switching of the branches during manipulation events triggered by the tip-molecule-substrate forces, as shown in Fig. 5a and b. A double switch from *open* to *trans-closed* and the back-switch of *trans-closed* to *open* is shown in Fig. 5c. This reversible switching confirms the full active functionality of **3** on the Ag(111) surface. Importantly, the dI/dV spectra of the switched forms have the same spectroscopic features as those shown in Fig. 4a, confirming the MnPc capability to undergo open/close isomerization while keeping the ligands structurally intact.

We also tested the use of bias pulses and slow ramps in the current or electric field to drive the molecular switches.[17,18,28,29] However, we discarded these methods since no changes were observed below a 3V threshold, whereas biasing the molecules above this value systematically led to non-reversible structural changes of the branches, in the form of dehydrogenation with the appearance of **4**-type branches (see ESI Fig. S6†).

Magnetic fingerprint of isomeric MnPcs

The second condition that we previously mentioned for the pathway to generate magneto-optical transducers is that our isomeric MnPc carries a well-defined magnetic moment. Based on previous work,[21,22] such properties can be validated through the detection of a Kondo effect on the Mn central atom. In MnPcs, the fingerprint of the Kondo effect has been identified by other groups as a resonance at the Fermi level with a linewidth of 13 meV convoluted with the Mn $d_{xz/yz}$ orbitals (characteristic of the D_{4h} squared planar symmetry group) appearing at −50 mV.[9,21,22] Therefore, using high-resolution dI/dV spectra in proximity of the Fermi energy we should verify the existence of the Kondo feature. The experimental data are shown in the inset of Fig. 4a. Indeed, our Mn STS reproduces the expected deconvolution analysis (see ESI Fig. S7d†), which can also be considered a further evidence of the correct MnPc formation by OSS.

DFT theory sheds light on the origin of this Kondo resonance that we locate at the pyrrole ring center, in agreement with previous work.[21,22] The calculated density of states pro-

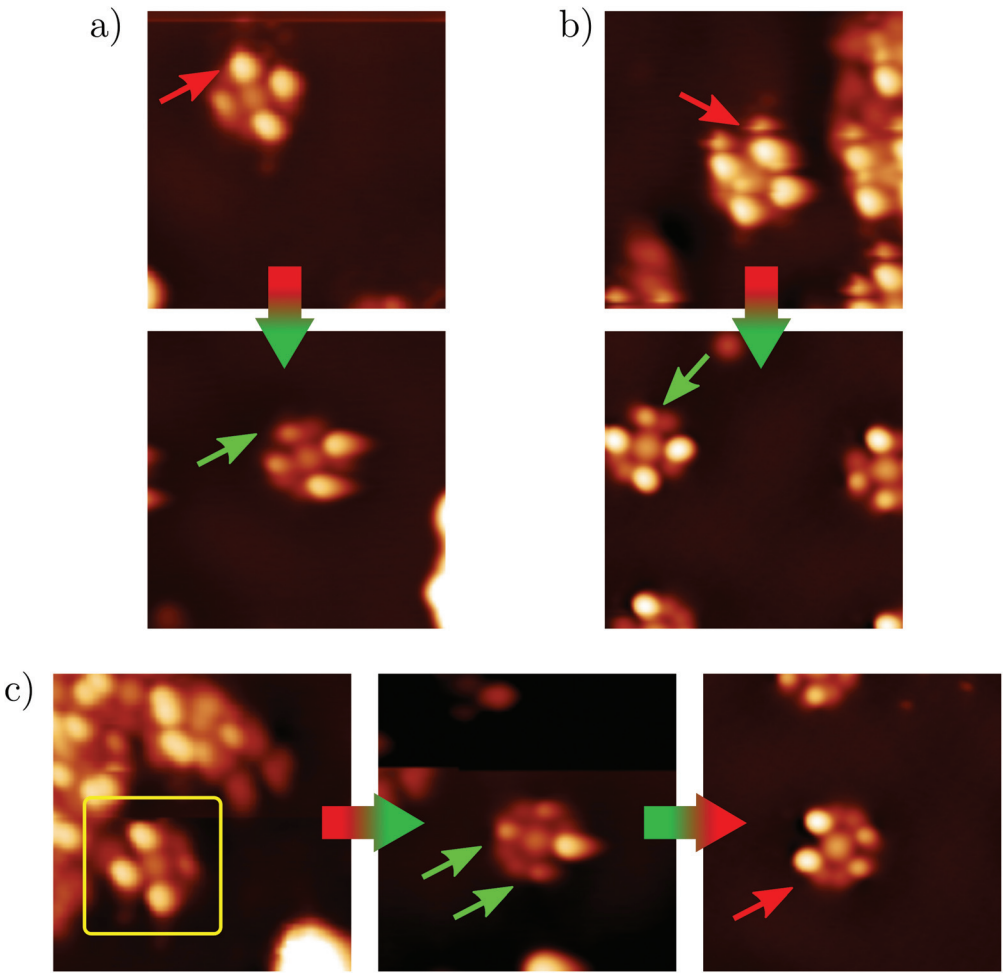

Fig. 5 Mechanical switching of the DAE moieties by tip manipulation. STM images recorded before and after the controlled lateral drag of **3** over the Ag surface (−100 mV, 50 pA, 8.75 × 8.75 nm^2). The arrows point to the switched branches. In the case of (a) and (b) one DAE branch changes from the *open* to *trans-closed* configuration. Alternatively, the sequence in (c) shows a reversible switch.

jected onto the Mn d orbitals indicate that the $d_{x^2-y^2}$ orbital is emptied, whereas the other four d orbitals are partially filled (see ESI Fig. S10†). This electronic arrangement results in a total magnetic moment slightly less than $2\mu_B$ where the main contribution is associated with the Mn center but with an opposite magnetic contribution from the molecular framework. Previously, the Kondo resonance was associated with the many-body screening of the d_{z^2} orbital by the conduction electrons of the substrate,[21] which in our case is substantiated by the nearly half-filling observed for this orbital. Also, the degenerated $d_{xz/yz}$ orbitals exhibit a strong contribution just below the Fermi level, accounting for the tail to the left of the Kondo resonance.

A critical parameter for the Kondo state is the screening strength, which affects the Kondo temperature and resonance line shape when, for instance, altering the distance of the central Mn to the metallic substrate. Despite the possibility of switching the branch configurations between *open* and *trans-closed*, we experimentally find for our switchable MnPcs that the low energy Mn spectra do not change (*cf.* ESI Fig. S7†). This can be understood if the Mn vertical distance turns out to be insensitive to the branch configuration, as deduced by theory (*cf.* Δz_{Mn} in Table 1). Furthermore, the identical planar environment of the Mn atoms in both configurations leads to nearly the same d orbital decomposition (ESI Fig. S10†). The use of bulkier groups at the hydrogen positions that are still optically active could lead to significant Mn height changes when switching between different open/closed isomers, thereby bearing the prospect of fulfilling the magnetic transducer functionality.

III. Conclusions

We have demonstrated that the branches of individual MnPc synthesized on Ag(111) can be mechanically switched between *open* and *trans-closed* isomeric forms. Preparation of the molecular complex has been possible by the OSS of a smaller precursor (**1**), which exhibits optical activity in solution, but most importantly maintains its integrity upon UHV sublimation. Indeed, the assignment of the two distinct configurations (open and closed atomic arrangements) was possible by combining STM images, STS spectroscopy and DFT calculations. Notably, we demonstrate the prospect of active functionality of these DAE branches by the configuration switching using tip manipulation processes. We also find that the Mn ions of **3** exhibits a significant magnetic fingerprint, so an entirely new playground to fabricate individually addressable magneto-optical transducers at the atomic scale is envisioned and requires further experimental validation.

The flexibility of the OSS process to produce complex structures, where the optical activity is brought by diarylethylene (DAE) moieties and the magnetism by metal centers exchangeable by metallation, opens vast opportunities. For instance, we foresee the implementation of different readout signals changing the magnetic state of the ion, the magneto crystalline anisotropy,[30,31] the energy resolved spin polarization of the local DOS,[32,33] or the Kondo screening.[21,22] Also, we envision the use of bulkier ligands to alter the adsorption geometry and height of the pyrrole ring around the metal center, thereby correlating the Kondo resonance to the different combinations of isomer ligands. All these possibilities expand the well-stablished spin-crossover photo-magnetism approach at the individual molecular level.

Author contributions

A. D.-C. and D. S. conducted the experiment and its data analysis; C. G.-F., P. K. and D. S.-P. performed the DFT calculations; S. Q. and D. P. designed and synthesized and purified the precursor molecules; and A. D.-C., D. S. and J. L.-C. wrote the manuscript. All authors contributed to the revision and final discussion of the manuscript.

Conflicts of interest

The authors declare no competing financial interests.

Acknowledgements

We sincerely thank Marten Piantek and Carlos Casas for their contribution to this work. Dr Piantek is also acknowledged for providing ideas for this work and for in-depth discussions. We gratefully acknowledge financial support from the Spanish Ministries of Economy, Industry and Competitiveness (MINECO, grants MAT2016-78293-C6-4-R and MAT2016-78293-C6-6) and of Science and Innovation (MICINN, grant no. PID2019-107338RB-C62, PID2019-107338RB-C64, PID2019-107338RB-C66/AEI/10.13039/501100011033 and RED2018-102833-T), the regional Governments of Aragon (E13-20R and E12-20R), the Xunta de Galicia (Centro de Investigación de Galicia acreditation 2019–2022, ED431G 2019/03), the Dept. of Education of the Basque Government and UPV/EHU (grant no. IT1246-19), the Spanish Research Agency (AEI), the European Regional Development Fund (ERDF) under the program Interreg V-A España-Francia-Andorra (contract no. EFA194/16 TNSI) and the European Union through Horizon 2020 (FET-Open project SPRING grant. no. 863098). Finally, we acknowledge support of the publication fee by the CSIC Open Access Publication Support Initiative through its Unit of Information Resources for Research (URICI).

Notes and references

1 O. Kahn and C. J. Martinez, *Science*, 1998, **279**, 44–48.
2 V. A. Dediu, L. E. Hueso, I. Bergenti and C. Taliani, *Nat. Mater.*, 2009, **8**, 707–716.
3 W. J. M. Naber, S. Faez and W. G. van der Wiel, *J. Phys. D: Appl. Phys.*, 2007, **40**, R205–R228.

4 H. Lu and N. Kobayashi, *Chem. Rev.*, 2016, **116**, 6184–6261.
5 J. M. Gottfried, *Surf. Sci. Rep.*, 2015, **70**, 259–379.
6 W. Auwärter, D. Écija, F. Klappenberger and J. V. Barth, *Nat. Chem.*, 2015, **7**, 105–120.
7 N. Tsukahara, K.-i. Noto, M. Ohara, S. Shiraki, N. Takagi, Y. Takata, J. Miyawaki, M. Taguchi, A. Chainani, S. Shin and M. Kawai, *Phys. Rev. Lett.*, 2009, **102**, 167203.
8 L. Gao, W. Ji, Y. B. Hu, Z. H. Cheng, Z. T. Deng, Q. Liu, N. Jiang, X. Lin, W. Guo, S. X. Du, W. A. Hofer, X. C. Xie and H.-J. Gao, *Phys. Rev. Lett.*, 2007, **99**, 106402.
9 K. J. Franke, G. Schulze and J. I. Pascual, *Science*, 2011, **332**, 940–944.
10 J. Kügel, M. Karolak, A. Krönlein, D. Serrate, M. Bode and G. Sangiovanni, *npj Quantum Mater.*, 2018, **3**, 53.
11 C. Wäckerlin, D. Chylarecka, A. Kleibert, K. Müller, C. Iacovita, F. Nolting, T. A. Jung and N. Ballav, *Nat. Commun.*, 2010, **1**, 61.
12 K. Seufert, W. Auwärter and J. V. Barth, *J. Am. Chem. Soc.*, 2010, **132**, 18141–18146.
13 C. F. Hermanns, M. Bernien, A. Krüger, W. Walter, Y.-M. Chang, E. Weschke and W. Kuch, *Phys. Rev. B: Condens. Matter Mater. Phys.*, 2013, **88**, 104420.
14 A. Köbke, F. Gutzeit, F. Röhricht, A. Schlimm, J. Grunwald, F. Tuczek, M. Studniarek, D. Longo, F. Choueikani, E. Otero, P. Ohresser, S. Rohlf, S. Johannsen, F. Diekmann, K. Rossnagel, A. Weismann, T. Jasper-Toennies, C. Näther, R. Herges, R. Berndt and M. Gruber, *Nat. Nanotechnol.*, 2020, **15**, 18–21.
15 N. Katsonis, T. Kudernac, M. Walko, S. J. van der Molen, B. J. van Wees and B. L. Feringa, *Adv. Mater.*, 2006, **18**, 1397–1400.
16 S. V. Snegir, P. Yu, F. Maurel, O. L. Kapitanchuk, A. A. Marchenko and E. Lacaze, *Langmuir*, 2014, **30**, 13556–13563.
17 M. Alemani, M. V. Peters, S. Hecht, K.-H. Rieder, F. Moresco and L. Grill, *J. Am. Chem. Soc.*, 2006, **128**, 14446–14447.
18 G. Reecht, C. Lotze, D. Sysoiev, T. Huhn and K. J. Franke, *ACS Nano*, 2016, **10**, 10555–10562.
19 P. Liljeroth, J. Repp and G. Meyer, *Science*, 2007, **317**, 1203–1206.
20 B.-Y. Choi, S.-J. Kahng, S. Kim, H. Kim, H. W. Kim, Y. J. Song, J. Ihm and Y. Kuk, *Phys. Rev. Lett.*, 2006, **96**, 156106.
21 J. Kügel, M. Karolak, J. Senkpiel, P.-J. Hsu, G. Sangiovanni and M. Bode, *Nano Lett.*, 2014, **14**, 3895–3902.
22 R. Tuerhong, F. Ngassam, S. Watanabe, J. Onoe, M. Alouani and J.-P. Bucher, *J. Phys. Chem. C*, 2018, **122**, 20046–20054.
23 M. Irie, *Chem. Rev.*, 2000, **100**, 1685–1716.
24 M. Piantek, D. Serrate, M. Moro-Lagares, P. Algarabel, J. I. Pascual and M. R. Ibarra, *J. Phys. Chem. C*, 2014, **118**, 17895–17899.
25 M. Koudia and M. Abel, *Chem. Commun.*, 2014, **50**, 8565–8567.
26 J. Wirth, N. Hatter, R. Drost, T. R. Umbach, S. Barja, M. Zastrow, K. Rück-Braun, J. I. Pascual, P. Saalfrank and K. J. Franke, *J. Phys. Chem. C*, 2015, **119**, 4874–4883.
27 S. Kezilebieke, A. Amokrane, M. Abel and J.-P. Bucher, *J. Phys. Chem. Lett.*, 2014, **5**, 3175–3182.
28 L. Grill, K.-H. Rieder, F. Moresco, S. Stojkovic, A. Gourdon and C. Joachim, *Nano Lett.*, 2006, **6**, 2685–2689.
29 X. H. Qiu, G. V. Nazin and W. Ho, *Phys. Rev. Lett.*, 2004, **93**, 196806.
30 A. F. Otte, M. Ternes, K. von Bergmann, S. Loth, H. Brune, C. P. Lutz, C. F. Hirjibehedin and A. J. Heinrich, *Nat. Phys.*, 2008, **4**, 847–850.
31 C. F. Hirjibehedin, C.-Y. Lin, A. F. Otte, M. Ternes, C. P. Lutz, B. A. Jones and A. J. Heinrich, *Science*, 2007, **317**, 1199–1203.
32 F. Meier, L. Zhou, J. Wiebe and R. Wiesendanger, *Science*, 2008, **320**, 82–86.
33 D. Serrate, P. Ferriani, Y. Yoshida, S.-W. Hla, M. Menzel, K. von Bergmann, S. Heinze, A. Kubetzka and R. Wiesendanger, *Nat. Nanotechnol.*, 2010, **5**, 350–353.